Improved watershed analysis for segmenting contacting particles of coarse granular soils in volumetric images

Article *in* Powder Technology · December 2019

DOI: 10.1016/j.powtec.2019.08.028

CITATIONS
9

READS
403

3 authors:

Quan Sun
Clemson University
19 PUBLICATIONS **77** CITATIONS
SEE PROFILE

Junxing Zheng
Iowa State University
71 PUBLICATIONS **606** CITATIONS
SEE PROFILE

Cheng Li
Chang'an University
19 PUBLICATIONS **105** CITATIONS
SEE PROFILE

Powder Technology 356 (2019) 295–303

Contents lists available at ScienceDirect

Powder Technology

journal homepage: www.elsevier.com/locate/powtec

Improved watershed analysis for segmenting contacting particles of coarse granular soils in volumetric images

Quan Sun [a], Junxing Zheng [a,*], Cheng Li [b]

[a] Department of Civil, Construction and Environmental Engineering, Iowa State University, Ames, IA 50011, USA
[b] Key Laboratory for Special Area Highway Engineering of Ministry of Education, School of Highway, Chang'an University, South 2nd Ring Road, Xi'an, Shanxi Province 710064, China

ARTICLE INFO

Article history:
Received 4 March 2019
Received in revised form 10 August 2019
Accepted 14 August 2019
Available online 16 August 2019

Keywords:
Granular soils
Watershed analysis
X-ray computed tomography
Image segmentation
Size and shape characterization

ABSTRACT

The watershed analysis has been widely used to segment contacting particles in volumetric images obtained from X-ray Computed Tomography (X-ray CT). However, the watershed analysis cannot discriminate between contacts of two particles and "necks" of peanut-shaped particles. Then, peanut-shaped particles are mistakenly oversegmented as two particles. To addresses this issue, this study developed an improved watershed analysis, which defines a dimensionless parameter α to discriminate contacts and necks. An image morphological reconstruction technique was developed to modify the distance map based on the parameter α. The watershed transform was performed on a modified distance map to overcome oversegmentation. The accuracy and effectiveness of the proposed technique were validated by six sand specimens. The influence of oversegmentation on particle size and shape characterizations were also demonstrated. The results showed that the improved 3D watershed analysis can effectively segment 3D particle contacts while preserving the continuity of necks for different granular soils.

1. Introduction

The image-based characterizations of soil particle shape and soil fabric are shifting from two-dimensional (2D) analysis to three-dimensional (3D) analysis. This trend has been witnessed by remarkable increases in studies that used 3D imaging techniques in the last five years. Many 3D imaging techniques have been adopted by geotechnical engineers for analyzing 3D particle sizes and shapes of granular soils, such as X-ray Computed Tomography (X-ray CT) [1–6], laser scanning technique [7–9], optical interferometer [10,11], stereophotography [12–14], and structured light technique [15]. Among these techniques, the X-ray CT technique gained the most extensive usage by geotechnical and material engineers because it can penetrate solids to capture internal structures of granular soils.

Druckrey et al. [1] and Kong and Fonseca [6] used X-ray CT to investigate 3D inter-particle contacts and the morphology of sands. Lim et al. [2], Jerves et al. [16], Zhou et al. [4], and Zhou and Wang [5] used X-ray CT to scan a limited number of soil particles and used the morphology characteristics of the scanned particles to generate realistic 3D particle analogs for discrete element modeling. Kawamoto et al. [17], Vlahinić et al. [18], and Fonseca et al. [19] performed X-ray CT scan on soil specimens during triaxial tests to investigate fabric evolutions of the specimens. Alam et al. [20], Imseeh et al. [21], and Mahbub and Haque [22] investigated the evolution of fabric anisotropy of sands during oedometer tests, and Soriano et al. [23] used X-ray CT to analyze the fabric of fiber-reinforced sands. Particle breakage characteristics of sands during uniaxial compression tests were also evaluated using X-ray CT by Cil and Alshibli [24] and Cil et al. [25]. Wiebicke et al. [26,27] investigated the effects of X-ray CT image resolution on particle contacts and their long axis characterizations.

The X-ray CT generates a volumetric image of a soil specimen, in which air voids have low grayscale values, and solid particles have high grayscale values. A threshold technique, such as Otsu's algorithm [28], can be used to convert the grayscale image to a binary image to separate the air voids and solid particles. In the binary image, the air has a voxel value of zero, and solid particles have a voxel value of one. However, soil particles are contacting with each other. Therefore, segmenting the contacting particles and identifying boundaries of individual particles are the prerequisite to further analysis. The aforementioned X-ray CT studies commonly used a watershed analysis to segment contact particles.

The basic concept of watershed analysis is to detect the constrained areas in volumetric images based on the assumption that the constrained areas are contacts between two particles. Then, the watershed analysis segments the constrained areas as shown in Fig. 1. The watershed analysis can effectively separate a majority of natural sands

* Corresponding author.
E-mail addresses: quansun@iastate.edu (Q. Sun), junxing@iastate.edu (J. Zheng), cli@chd.edu.cn (C. Li).

https://doi.org/10.1016/j.powtec.2019.08.028
0032-5910/

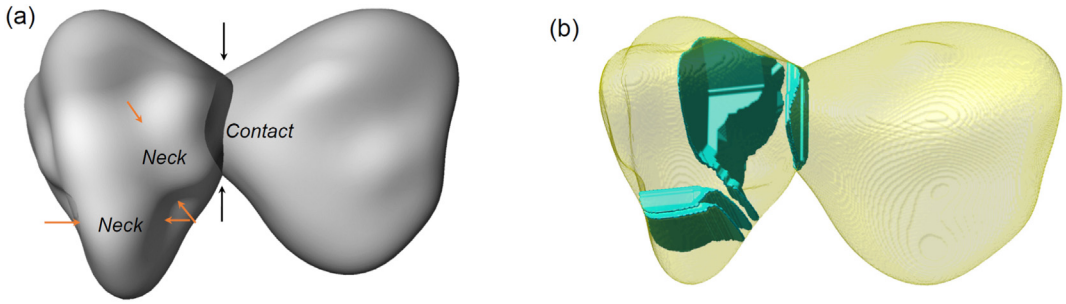

Fig. 1. Oversegmentation of peanut-shaped particles by original watershed analysis: (a) a volumetric image containing two natural soil particles that are contacting with each other, (b) oversegmentation of peanut-shaped particle by original watershed analysis.

with regular-shaped (i.e., spherical) particles. However, natural and crushed sands contain many peanut-shaped particles with constrained areas, which may be considered as the "necks" of the particles as shown in Fig. 1(a). The watershed analysis cannot discriminate between contacts and necks, and therefore, mistakenly segments peanut-shaped particles into two parts or even more parts as shown in Fig. 1(b). Without proper corrections, the oversegementation will adversely affect the subsequent analysis on the particle size and shape characterizations, fabric anisotropy, and inter-particle contacts, leading to misleading results [29].

Researchers have developed various techniques for eliminating oversegmentation of watershed analysis in 3D volumetric images. Faessel and Jeulin [30] proposed a stochastic watershed technique to eliminate the oversegmentation. A probabilistic density function was used to determine key parameters in the segmentation. Faessel and Jeulin [30] showed that this technique could ensure correct segmentations for regular-shaped particles, but they did not validate this technique on the soils with peanut-shaped particles. Alam and Haque [31] developed a cluster analysis marker controlled watershed method that used a cluster evaluation framework to segment contact particles. This technique can segment most regular- and peanut-shaped particles but was unsuccessful for some very elongated particles. To solve the problem, they also introduced a semi-automatic method to manually select and segment these unseparated particles. Alam and Haque's [31] method demonstrated a significant improvement of the original watershed analysis toward overcoming oversegmentation, but manual efforts were still required. In volumetric images containing a large number of particles, it was challenging to inspect and identify very elongated particles.

Notable progress has been made by Kong and Fonseca [6] very recently. They developed an adaptive watershed analysis to overcome oversegmentation of peanut-shaped particles in shelly carbonate sands. The basic principle was to perform a series of iterations that enabled the segmentation to become progressively more refined. This technique showed remarkably accurate segmentation results for shelly carbonate sands containing many peanut-shaped particles. However, this method was complicated, computationally demanding, and requires operators to have a high level of image processing background to implement.

The motivation of this study is to develop a simple, fast, and accurate method to solve the oversegmentation issue of the watershed analysis. The key is to develop a dimensionless factor α to discriminate peanut-shaped particles and real contacting particles. Small α values are observed for peanut-shaped particles, while large α values are observed for contacts. Therefore, a threshold α value is searched by evaluating a large number of peanut-shaped particles and contacting particles. Then, a morphological reconstruction technique is introduced to improve the watershed analysis based on the threshold α value. The effectiveness and accuracy of the newly improved watershed analysis are validated by six sand specimens with various particle shapes.

2. Introduction to the watershed analysis and oversegmentation

The watershed analysis was proposed by Beucher and Lantuejoul [33]. The watershed analysis contains two steps: distance map transform and watershed transform. For an explanation of the idea, three binary spheres are used as an example in Fig. 2(a). The spheres A and B together represent a peanut-shaped soil particle. The sphere C represents a spherical particle. The peanut-shaped and spherical particles are contacting with each other. Fig. 2(a) has a size of $150 \times 150 \times 300$ voxels. The points inside the particles have a voxel value of one, and the points outside the particles have a voxel value of zero.

In the first step, a 3D Euclidean distance map is computed. For each voxel inside the particles, such as the point located at (x, y, z) in Fig. 2(a), the shortest distance to the background (the zero voxels) is computed as D(x, y, z), which is a decimal floating-point number. After calculating the shortest distances for all the points inside the particles, a 3D Euclidean distance map can be obtained, as shown in Fig. 2(b).

In the second step, the watershed transform is performed on the Euclidean distance map. The Euclidean distance map can be considered as a topographic map consisting of ridges and basins as shown in Fig. 3(a). The points with the maximum distance value create local minima of the basins, while the shallower points between two local minima create the ridges. The ridges corresponding to contacts are defined as contact ridges, and the ridges corresponding to necks are defined as neck ridges as shown in Fig. 3(a). The watershed transform can be thought of as gradually injecting water into the basins through the local minima points. The water table rises uniformly as shown in Fig. 3(a), and the water from two basins eventually meet at the ridges as shown in Fig. 3(b). Each constrained region generates a ridge resulting in a segmentation. The watershed transform separates particles at all of the ridges in the image as shown in Fig. 3(c).

The constrained regions could be contacts between two particles or necks of peanut-shaped particles. Both types of constrained regions can generate ridges, so the watershed analysis cannot discriminate these two types of ridges, leading to oversegmentation at necks as shown in Fig. 3(b) and (c). To effectively avoid oversegmentation, neck ridges (false contacts) must be distinguished from contact ridges (real contacts between particles).

3. Discrimination between necks and contacts

By looking at the contacting particles in Fig. 3(c), an observer can easily discriminate between necks and contacts. In human's cognitive process, we essentially compare the sizes (or areas) of constrained regions: the contacts usually have relatively smaller constrained regions than the necks. Based on the inspiration of the human cognitive process, this study developed an automated algorithm to discriminate between necks and contacts of particles.

Two spheres with radii of R_1 and R_2 are used to illustrate the concept in Fig. 4(a). Those two spheres could be either two contacting particles or a single peanut-shaped particle. The constrained region is a circle

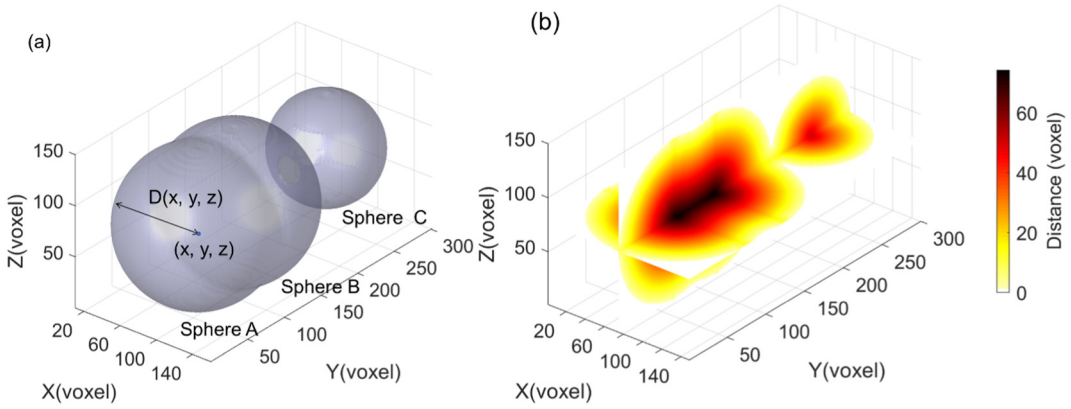

Fig. 2. Illustration of the distance transform: (a) two contacting particles (spheres A and B composite a peanut-shaped particles, and sphere C is a spherical particle), (b) the 3D Euclidean distance map by the distance transform.

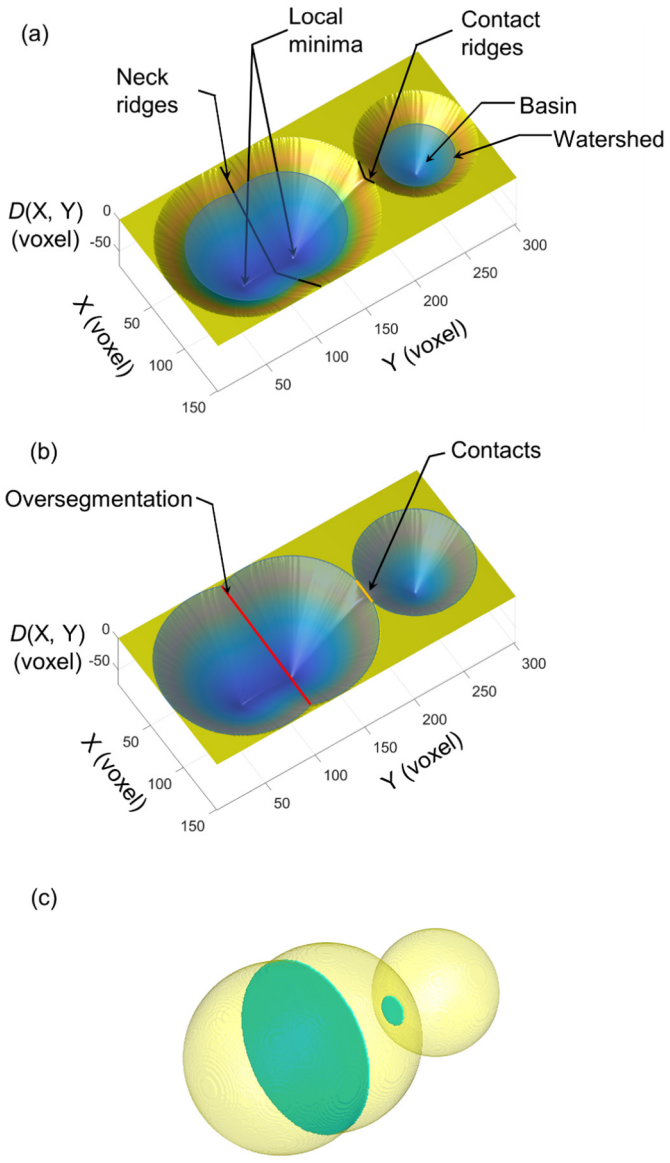

Fig. 3. Illustration of the watershed transform: (a) converting the 3D Euclidean distance to a topographic map; (b) illustration of watershed transform by injecting water into the basins through the local minima points; (c) oversegementation caused by watershed analysis.

with a radius of r. A dimensionless factor α is defined to quantify the size of the constrained region:

$$\alpha = \frac{h}{R_2} = 1 - \frac{r}{R_2} \tag{1}$$

$$h = R_2 - r \tag{2}$$

The h is the difference between the radius of the constrained circle r and the radius of the smaller sphere R_2, which is essentially the height of ridge relative to the shallower minima. The α varies from 0 to 1 as shown in Fig. 5(a) to (f). The radius of constrained regions decreases as increasing α values. Therefore, for small α values, two spheres look more like a peanut-shaped particle. For large α values, two spheres look more like two contacting particles.

Natural soil particles may not be spherical shapes, so the constrained regions may not be a circle. Therefore, the particle sizes (R_1 and R_2) and constrained region size (r) should be redefined for soil particles with irregular shapes. There were many ways to define these values. For example, the R_1 and R_2 could be generalized as the radii of the maximum inscribed spheres or the minimum circumscribing spheres of two contacting particles or two parts of a peanut-shaped particle. The R_1 and R_2 could also be generalized as the radii of spheres having the same volumes or surface areas as two contacting particles or two parts of a peanut-shaped particle. The r could be generalized as the radius of the circle having the same area as the constrained region, or the radius of the circle having the same perimeter as the constrained region, or the radius of the maximum inscribed circle of the constrained region, or the radius of the minimum circumscribing circle of the constrained region.

In this study, the R_1 and R_2 values were defined as the radii of the maximum inscribed spheres of two contacting particles or two parts of a peanut-shaped particle because of the easiness of determining these values. The R_1 and R_2 values can be determined from the Euclidean distance map. The maximum values of the distance map (or the local minima of the basins in the topographic map) of irregular soil particles identify the R_1 and R_2 values. The r was defined as the radius of a circle with the same area as the constrained region because we found that this definition yielded best results for discriminating necks and contacts.

To investigate α values of peanut-shaped particles and two contacting particles, we manually selected 5000 peanut-shaped and elongated particles in the range of 2.0 to 35.0 mm from ten different silica sands including five crushed sands and five natural sands. An EinScan-SP 3D laser scanner was used to scan the selected particles. The maximum scanning volume of EinScan-SP scanner is 200 × 200 × 200 mm, and the scanning accuracy is 0.05 mm. Having the 3D geometries, the α values of those 5000 particles were computed.

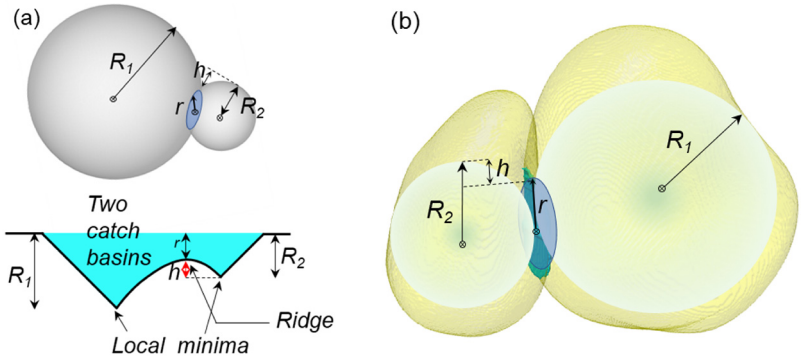

Fig. 4. Definition of the dimensionless parameter α: (a) the definition of α based on idealized spheres, (b) the definition of α based on realistic particles.

The spherical particles without necks have $\alpha = 0$ as shown in Fig. 5 (Particles #1, #7, and #13). The necks of most peanut-shaped particles were smaller than 0.16. Six peanut-shaped particles having $\alpha = 0.07$ and 0.16 are shown in Fig. 5 (Particles #2, #3, #8, #9, #14, and #15). We also scanned various contacting particles and computed their α values. The results showed that α values of most contacts were larger than 0.20. Nine pairs of contacting particles having $\alpha = 0.20$, 0.50, and 1.0 are shown in Fig. 5 (Particles #4 to #6, #10 to #12, and #16 to #18).

We observed that some peanut-shaped particles had α values as large as 0.20 while some contacting particles had α values as small as 0.16, such as particles No. 19 and No. 20 in Fig. 5. However, these cases are very rare in silica sands. Therefore, in this study, the $\alpha_0 = 0.16$ is selected as the threshold value to discriminate between necks and contacts. It should be noted that $\alpha_0 = 0.16$ is applicable to discriminate necks and contacts for commonly used silica sands. We did not evaluate α values of other special sands, such as shelly carbonate sands containing a large amount of marine organisms (e.g., shells and skeletal particles). The readers should calibrate a new α_0 for these special sands. Having discriminating necks and contacts, the next question is how to eliminate segmentations at necks and preserve segmentations at contacts.

4. Improving watershed analysis to overcome oversegmentation

As established above, neck ridges in the distance map can cause oversegmentation during the watershed transform. Therefore, if the distance map could be modified to eliminate those neck ridges, oversegmentation would be eliminated. One possible method is to elevate the local minima until the heights of neck ridges become zeros. Then, only contact ridges show up in the distance map. The watershed transform will only segment contacts.

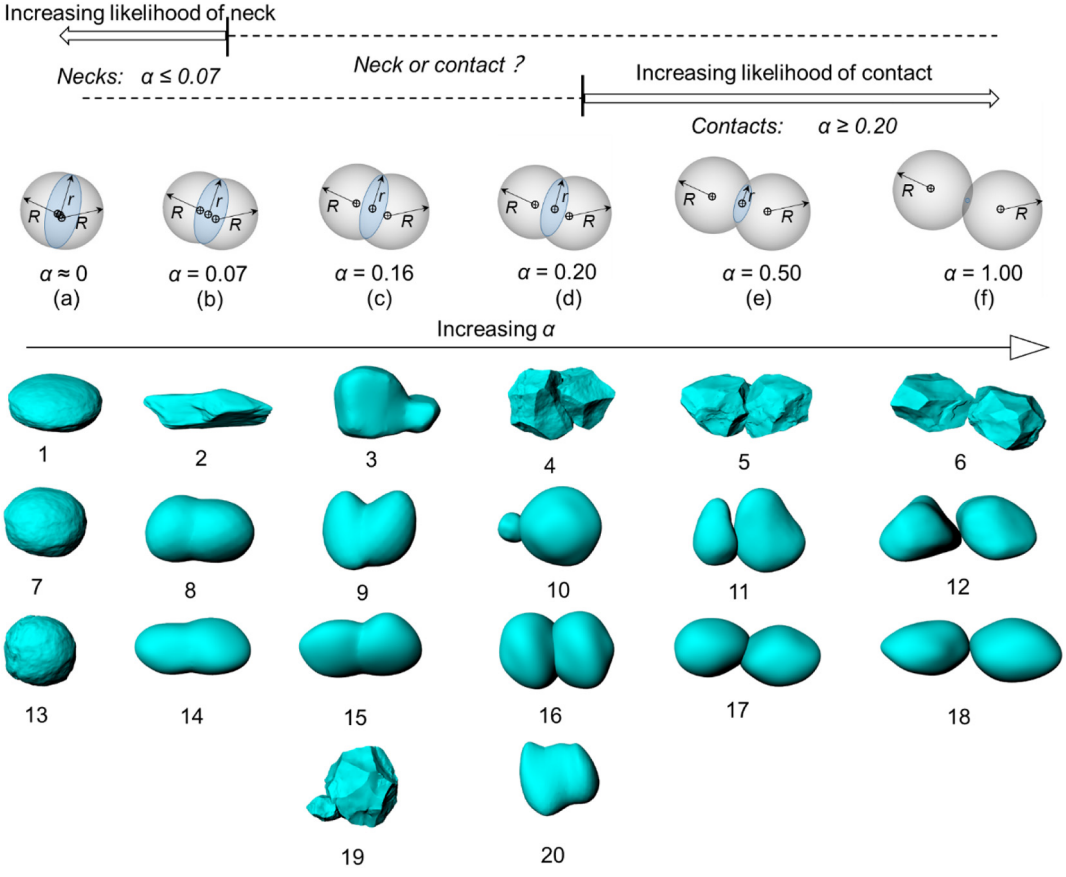

Fig. 5. The α values of some evaluated soil particles in this study.

The particles in Fig. 6(a) is used to illustrate the idea. The slice of the distance map that cuts through centers of three spheres is shown in Fig. 6(b). Three local minima and two ridges are observed. The ridge 1 is the neck ridge with $\alpha = 0.10$, which is below the threshold 0.16. The ridge 2 is a contact ridge with $\alpha = 0.63$, which is larger than the threshold 0.16. Due to the existence of the two ridges, the watershed algorithm will segment these particles into three particles. The peanut-shaped particle will be oversegmented.

The oversegmentation can be eliminated by elevating the local minima in the distance map following the equation:

$$\Delta R = \begin{cases} \alpha_0 R & \text{if R was not used to compute the } \alpha \text{ of any ridge} \\ min(\alpha_0 R, \alpha R) & \text{if R was used to compute the } \alpha \text{ of any ridge} \end{cases} \quad (3)$$

where ΔR is the increment by which the bottoms of local minima is elevated; R is the depth of the local minima, which is equal to radii of spheres; the α is computed using Eq. (1); and the $\alpha_0 = 0.16$ is the previously determined threshold value between necks and contacts.

The local minima in Fig. 6(b) are uplifted using Eq. (2). The computational process is following. The local minimum R_1 is not used for calculating the α of any ridge. Therefore, the elevation of R_1 is $\Delta R_1 = 0.16R_1$. The local minimum R_2 is used to compute α_1 in Fig. 6(b) Therefore, the R_2 is uplifted by $\Delta R_2 = \min(0.16R_2, 0.10\ R_2) = 0.10\ R_2$. The local minimum R_3 is used to compute α_2 in Fig. 6(b). Therefore, the R_3 is uplifted by $\Delta R_3 = \min(0.16R_3, 0.63R_3) = 0.16\ R_3$. Then the distance map is modified in Fig. 6(c).

In the modified distance map, neck ridge (ridge 1) disappears, and the contact ridge (ridge 2) is unaffected. Therefore, the peanut-shaped particle (particle 1) has only one local minimum. If the watershed transform is performed on the modified distance map, it will only identify the contact ridge (ridge 2) and will not oversegment the peanut-shaped particle.

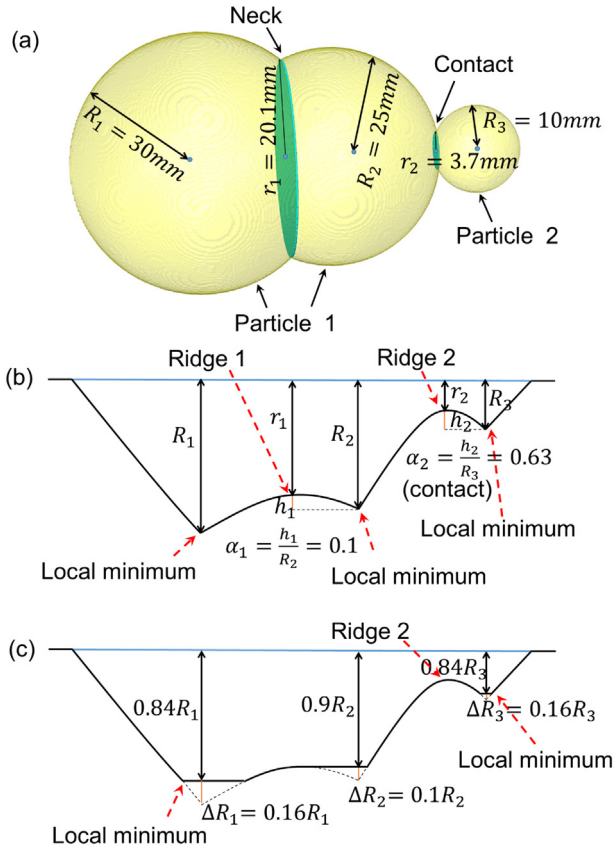

Fig. 6. The basic concept of the improved watershed analysis: (a) contacting particles oversegmentated by watershed analysis, (b) one slice of the 3D Euclidean distance map, and (c) the modified distance map based on eq. (3).

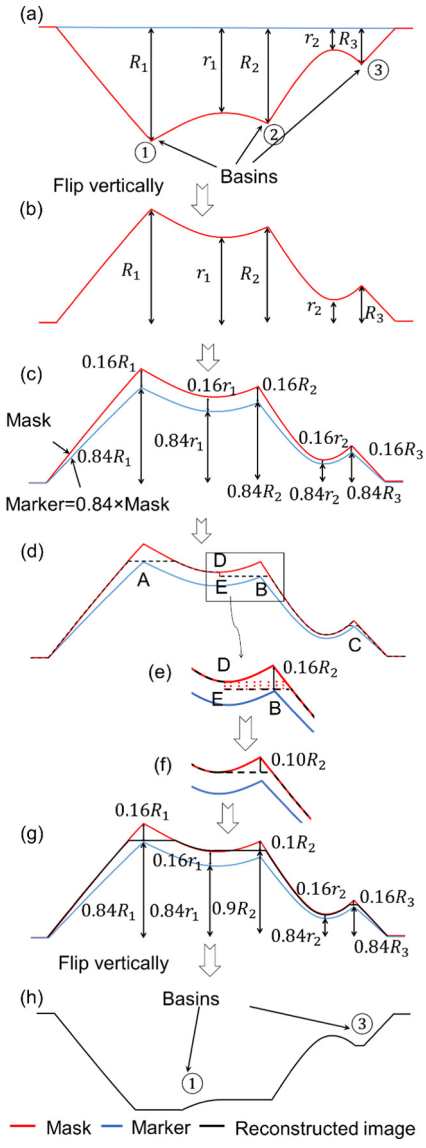

Fig. 7. Illustration of the 3D image morphological reconstruction algorithm for modifying the distance map: (a) the distance map replotted from Fig. 6(b), (b) the vertically flipped distance map, (c) mask and marker images determined by Eq. (3), (d), (e), and (f) morphological reconstruction process, (g) the reconstructed distance map, (h) the vertically flipped reconstructed distance map.

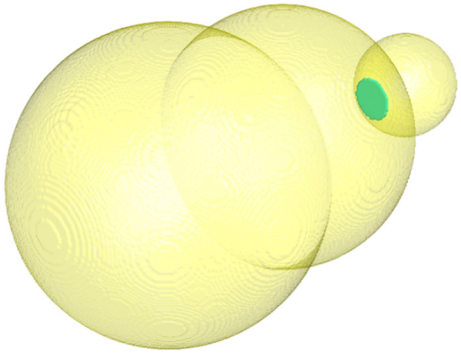

Fig. 8. The improved watershed analysis to eliminate the oversegemetation.

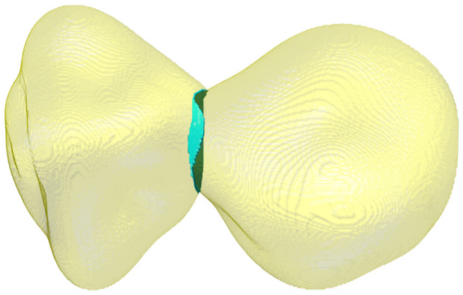

Fig. 9. The improved watershed analysis to eliminate the oversegemetation in natural soil particles.

5. 3D image morphological reconstruction

The morphological reconstruction can be used to modify the distance map based on the Eq. (3). The two particles in Fig. 6(a) and their distance map in Fig. 6(b) will be used herein to illustrate the concept of 3D image morphological reconstruction. The distance map in Fig. 6 (b) is replicated in Fig. 7(a) and then flipped vertically to generate a "mask" image in Fig. 7(b). The mask image multiplies $(1 - \alpha_0)$ ($\alpha_0 = 0.16$ as previously established) to generate a "marker" image in Fig. 7 (c). Every point on the marker image dilates horizontally until it encounters the mask as shown in Fig. 7(d). Such dilation process will not change the amplitudes of the peaks. Therefore, a "discontinuity," DE, is generated, which is magnified in Fig. 7(e). Due to unimpeded dilation from right, the DE will continue to dilate horizontally from left to right

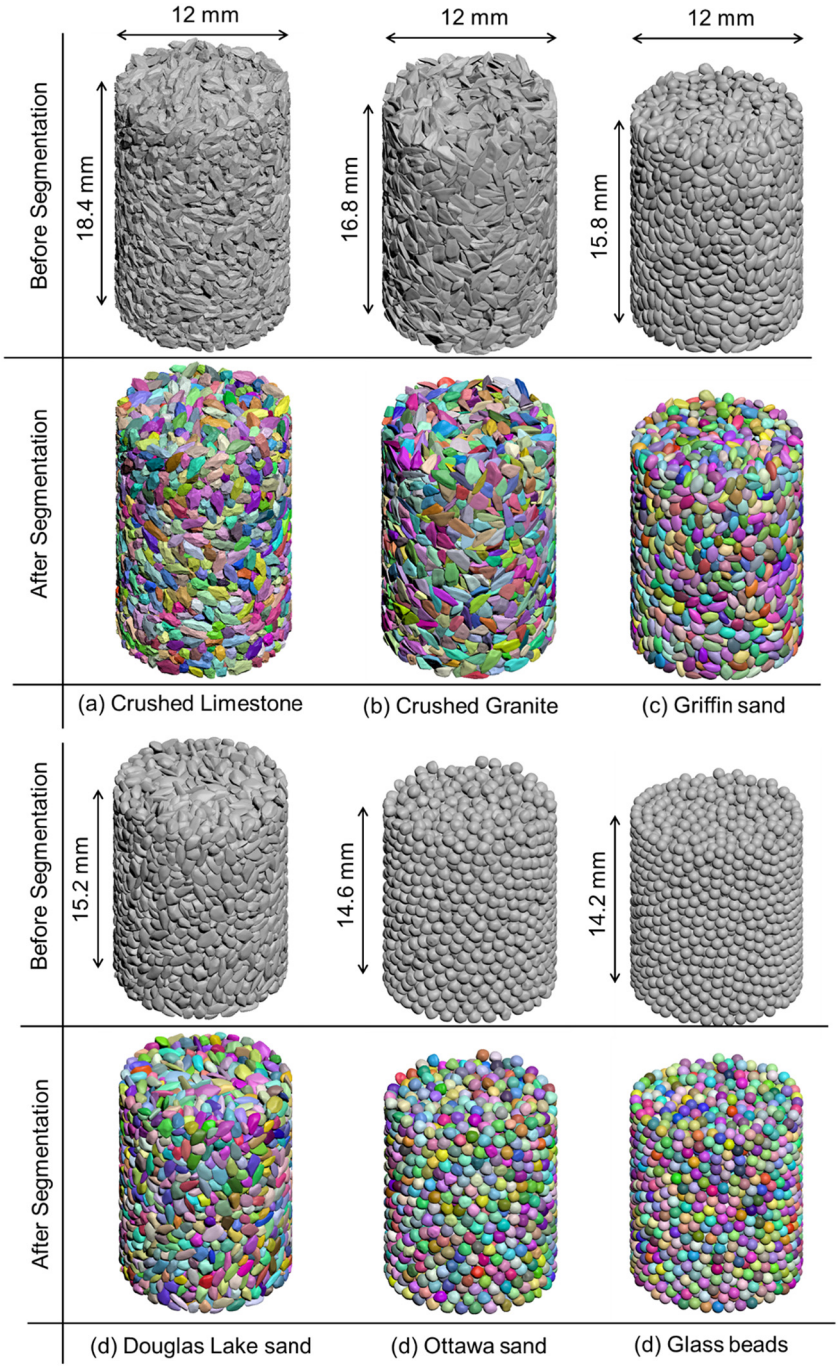

Fig. 10. Validation of the improved watershed analysis by six sand specimens.

until it encounters the marker as shown in Fig. 7(f). The reconstructed distance map is shown in Fig. 7(g). The vertically flipped reconstructed distance map is shown in Fig. 7(h), which is identical to the target distance map in Fig. 6(c). The watershed transform can now be performed on the reconstructed distance map. As expected, only one segmentation occurs at contact as shown in Fig. 8.

The 3D morphological reconstruction was used to modify the distance map of the particles showing in Fig. 1. The watershed transform was performed on the modified distance map. The result is shown in Fig. 9. Two particles were correctly segmented at their contact. The oversegmentation has been successfully eliminated.

6. Validation of the improved watershed analysis

Six sand specimens are used in this study to validate the proposed improved watershed analysis as shown in Fig. 10. They included crushed limestone (very angular particles), crushed granite (very angular to angular particles), Griffin sand (subangular to sub-rounded particles), Douglas lake sand (sub-rounded particles), Ottawa sand (rounded to well-rounded particles) and glass beads (well-rounded particles). For each sand, we manually picked 4000 particles in a range of #30 sieve (0.595 mm) to #18 sieve (1.00 mm). We purposely selected particles with flat, elongated, and peanut shapes for creating challenging scenarios for segmentations. However, Ottawa sand and glass beads included mainly spherical particles, so we randomly picked out 4000 particles from these two sands. These six sand specimens may be representative for commonly used sands in geotechnical research and practice. If the improved watershed analysis could correctively segment these challenging specimens, it will likely be successful for segmenting other natural sands with less flat, elongated, and peanut-shaped particles.

The selected particles were funneled into a 12 mm diameter plastic cylinder and were vibrated to generate dense specimens. A high-resolution X-ray Computed Tomography (X-ray CT) was used to scan specimens with a resolution of 10 μm/voxel, which yielded 3D volumetric images. The Otsu's [28] threshold technique was used to convert the grayscale image to a binary image to separate the air voids and solid particles. In the binary image, the air had a voxel value of zero, and solid particles had a voxel value of one. The solid particles before segmentation are shown in Fig. 10.

The 3D distance maps for the volumetric images were computed. The distance map was modified using the morphological reconstruction to eliminate the neck ridges. The α_0 was set as 0.16. The watershed transform was performed on the modified distance map. A total of 4000 particles were determined for each sand specimen. The segmented particles are plotted in different colors in Fig. 10. All particles were successfully separated, and no oversegemetation occurred. The results can validate the effectiveness and accuracy of the proposed watershed analysis.

7. Effects of oversegmentation on particle size and shape distributions

It is also interesting to see the effects of oversegmentation on the particle size and shape characterizations. To determine the particle size, three principal dimensions of a particle, including length (d_1), width (d_2), and thickness (d_3), must be determined. Druckrey et al. [1] showed that a PCA (principal component analysis) technique could rapidly and accurately determine d_1, d_2, and d_3 values of 3D particles. This technique was used in this study. A 3D soil particle is used to illustrate the concept of PCA as shown in Fig. 11. The PCA projects the vertices of the 3D particle into three orthogonal directions called three principal components. The first principal component is a direction having the largest possible variance of the data. It determines the d_1 of the 3D particle. The second principal component is a direction having the second-largest possible variance of the data but orthogonal to the first principal component. It determines the d_2 of the 3D particle. The third principal component is a direction having the third-largest possible variance of the data but orthogonal to the first and second principal components. It determines the d_3 of the 3D particle.

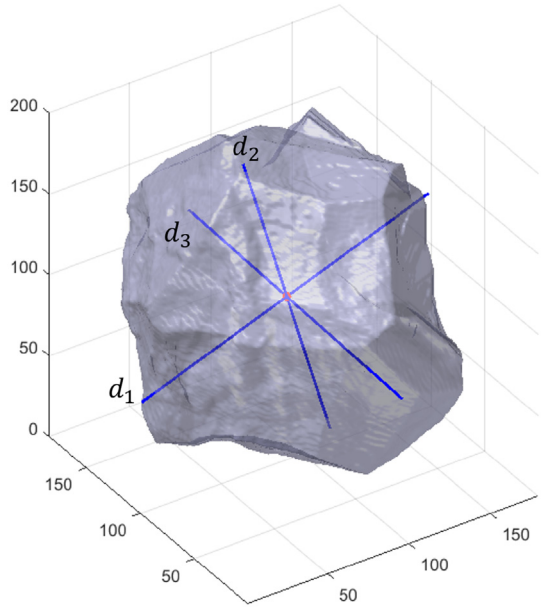

Fig. 11. Illustration of the principal component analysis (PCA).

Based on the three principal dimensions, Zheng and Hryciw [14] used an ellipsoid particle model to determine sieve equivalent particle size d_e:

$$d_e = \sqrt{\frac{d_2^2 + d_3^2}{2}} \tag{4}$$

The crushed limestone specimen was used as an example to illustrate the effects of oversegmentations. Correctly segmented particles in Fig. 10(a) were used to compute d_e values. The volume of each particle was computed as $d_1 \times d_2 \times d_3$. Therefore, the volume based d_e distribution is shown in Fig. 12. The sieving analysis results are also superimposed on Fig. 12. The optical and sieving-based particle size distributions agree well with each other.

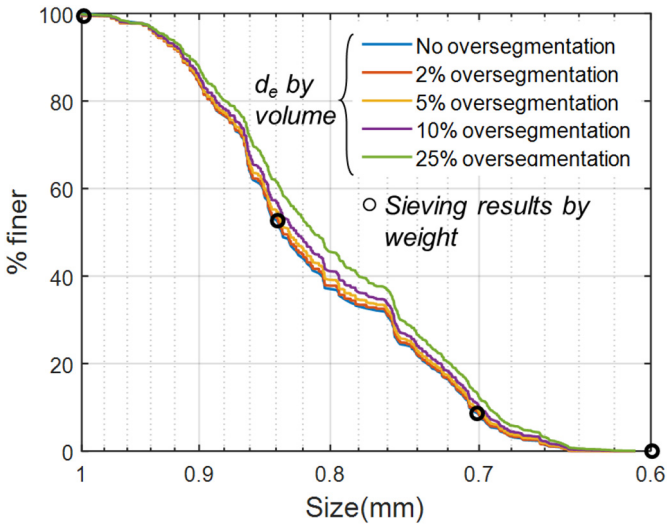

Fig. 12. Effects of oversegmentation on the particle size distributions.

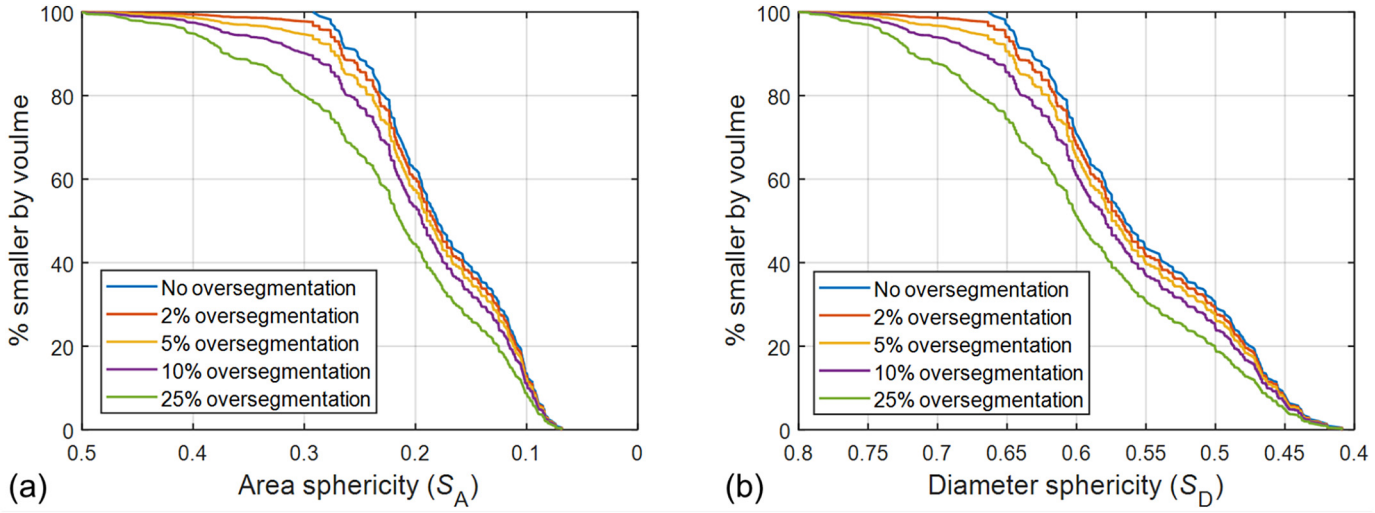

Fig. 13. Effects of oversegmentation on particle shape distributions.

We reduced α_0 values and performed improved watershed analysis on the crushed limestone specimen to generate oversegmentations. By adjusting the α_0 values, we ovesegmented 2% (81 particles), 5% (190 particles), 10% (420 particles), and 25% (1005) particles out of 4000 particles. Then, the particle size distributions of oversegmented specimens were recomputed, and the results are shown in Fig. 12. As expected, particle sizes are underestimated as a result of oversegmentation. However, 2% oversegmentation produced small effects on particle size distribution results.

This study used area sphericity proposed by Riley [32], and diameter sphericity proposed by Wadell [33] to characterize particle shape:

Area sphericity:

$$S_A = \frac{A}{A_{\text{cir}}} \tag{5}$$

Diameter sphericity:

$$S_D = \frac{D_e}{D_{\text{cir}}} \tag{6}$$

Where A is the area of the particle; A_{cir} is the area of the smallest circumscribing circle of the particle; D_e is the diameter of a circle having the same area as the original particle; D_{cir} is the smallest circumscribing circle of the particle. These parameters can be determined by the computational geometry algorithm developed by Zheng and Hryciw [34,35].

The area sphericity and diameter sphericity of crushed limestone specimen particles in Fig. 10 (a) were determined. Then volume-based particle shape distributions are plotted in Fig. 13(a) and (b). Oversegmented specimen by using different α_0 values were also analyzed, and the particle shape distributions were determined as shown in Fig. 13(a) and (b). As expected, particles were more spherical as a result of oversegmentation. However, 2% oversegementation produces small effects on particle shape distribution curves.

As discussed in Fig. 5, some peanut-shaped particles could occasionally have α_0 values larger than 0.20, while some contacting particles could occasionally have α_0 values smaller than 0.16. These particles are very rare in natural soils. For example, we did not find these abnormal particles in the six specimens in Fig. 10. Therefore, even if these abnormal particles exist in some sand specimens, they will likely have minor effects on particle size and shape distributions as long as the number of these particles are smaller than 2% of the number of analyzed particles.

8. Conclusion

The original watershed analysis identified all of the constrained areas in the 3D volumetric images and segmented those constrained areas, but those constrained areas could be contacts of two particles or necks of peanut-shaped particles. Therefore, the original watershed analysis may mistakenly segment peanut-shaped particles into two parts or even more parts, because it cannot discriminate between contacting particles and peanut-shaped particles.

In this study, the original watershed analysis was improved by incorporating a dimensionless parameter α to discriminate between contacts and necks. Small α values indicated that the constrained areas were more likely to be necks of a particle, and large α values indicated that the constrained areas were more likely to be contacts between particles. To determine the threshold α value for discriminating necks and contacts, a total of 5000 peanut-shaped and elongated particles were analyzed. The results indicated that the α values of particle necks were smaller than 0.16, while the α values of contacts were larger than 0.20. The oversegmentation issue can be addressed by modifying the distance map based on the threshold α value. The key concept was to uplift local minima until the heights of neck ridges became zeros, and only contact ridges showed up in the distance map. A 3D image morphological reconstruction was introduced to automate the distance map modification. This technique can generate the target distance map for performing the improved watershed transform.

To validate the accuracy and effectiveness of the improved watershed analysis, this technique was used to segment six sand specimens including crushed limestone (very angular particles), crushed granite (very angular to angular particles), Griffin sand (subangular to subrounded particles), Douglas lake sand (sub-rounded particles), Ottawa sand (rounded to well-rounded particles) and glass beads (well-rounded particles). The improved watershed analysis successfully eliminated oversegmentment in these sand specimens.

The effects of oversegmentation on particle size and shape characterizations were analyzed using the crushed limestone specimen. By adjusting the α_0 values used in the improved watershed analysis, we oversegmented 2%, 5%, 10%, and 25% particles out of 4000 particles. The results showed that 2% oversegementation produced small effects on particle size and shape distribution curves.

Acknowledgments

This material is based upon work supported by the U.S. National Science Foundation under Grant No. CMMI 1917332. Any opinions, findings, and conclusions or recommendations expressed in this material

are those of the authors and do not necessarily reflect the views of the National Science Foundation. The authors also want to acknowledge the Center of Nondestructive Evaluation, Iowa State University for their supports on X-ray Computed Tomography (CT) scans.

References

[1] A.M. Druckrey, K.A. Alshibli, R.I. Al-Raoush, 3D characterization of sand particle-to-particle contact and morphology, Comput. Geotech. 74 (2016) 26–35, https://doi.org/10.1016/j.compgeo.2015.12.014.
[2] K.-W.W. Lim, R. Kawamoto, E. Andò, G. Viggiani, J.E. Andrade, Multiscale characterization and modeling of granular materials through a computational mechanics avatar: a case study with experiment, Acta Geotech. 11 (2015) 243–253, https://doi.org/10.1007/s11440-015-0405-9.
[3] K.A. Alshibli, M.F. Jarrar, A.M. Druckrey, R.I. Al-Raoush, R.I. Al-Raoush, Influence of particle morphology on 3D kinematic behavior and strain localization of sheared sand, J. Geotech. Geoenviron. Eng. 143 (2017) 1–25, https://doi.org/10.1061/(asce)gt.1943-5606.0001601.
[4] B. Zhou, J. Wang, Random generation of natural sand assembly using micro x-ray tomography and spherical harmonics, Géotechn. Lett. 5 (2015) 6–11, https://doi.org/10.1680/geolett.14.00082.
[5] B. Zhou, J. Wang, Generation of a realistic 3D sand assembly using X-ray micro-computed tomography and spherical harmonic-based principal component analysis, Int. J. Numer. Anal. Methods Geomech. 41 (2016) 93–109, https://doi.org/10.1002/nag.2548.
[6] D. Kong, J. Fonseca, Quantification of the morphology of shelly carbonate sands using 3D images, Géotechnique. 68 (2018) 249–261, https://doi.org/10.1680/jgeot.16.P.278.
[7] H. Kim, C.T. Haas, A.F. Rauch, C. Browne, Dimensional ratios for stone aggregates from three-dimensional laser scans, J. Comput. Civ. Eng. 16 (2002) 175–183, https://doi.org/10.1061/(ASCE)0887-3801(2002)16:3(175.
[8] Y. Hayakawa, T. Oguchi, Evaluation of gravel sphericity and roundness based on surface-area measurement with a laser scanner, Comput. Geosci. 31 (2005) 735–741, https://doi.org/10.1016/j.cageo.2005.01.004.
[9] J.K. Anochie-boateng, J.J. Komba, G.M. Mvelase, Three-dimensional laser scanning technique to quantify aggregate and ballast shape properties, Constr. Build. Mater. 43 (2013) 389–398, https://doi.org/10.1016/j.conbuildmat.2013.02.062.
[10] M. Otsubo, C. O'sullivan, W.W. Sim, E. Ibraim, Quantitative assessment of the influence of surface roughness on soil stiffness, Géotechnique. 65 (2015) 694–700, https://doi.org/10.1680/geot.14.T.028.
[11] K.A. Alshibli, M.I. Alsaleh, Characterizing surface roughness and shape of sands using digital microscopy, J. Comput. Civ. Eng. 18 (2004) 36–45, https://doi.org/10.1061/~ASCE!0887-3801~2004!18:1~36!.
[12] J. Zheng, R.D. Hryciw, Soil particle size characterization by stereophotography, Geotech. Spec. Publ. (2014) https://doi.org/10.1061/9780784413272.007.
[13] J. Zheng, R. Hryciw, H.-S. Ohm, Three-dimensional translucent segregation table (3D-TST) test for soil particle size and shape distribution, Geomech. Micro Macro (2014) 1037–1042, https://doi.org/10.1201/b17395-186.
[14] J. Zheng, R.D. Hryciw, Soil particle size and shape distributions by stereophotography and image analysis, Geotech. Test. J. 42 (2017) 1–14, https://doi.org/10.1520/GTJ20160165.
[15] Q. Sun, Y. Zheng, B. Li, J. Zheng, Z. Wang, Three-dimensional particle size and shape characterization using structural light, Geotech. Lett. 9 (2019) 1–7, https://doi.org/10.1680/jgele.18.00207.
[16] A.X. Jerves, R.Y. Kawamoto, J.E. Andrade, A geometry-based algorithm for cloning real grains, Granul. Matter 19 (2017) 1–10, https://doi.org/10.1007/s10035-017-0716-7.
[17] R. Kawamoto, E. Andò, G. Viggiani, J.E. Andrade, Level set discrete element method for three-dimensional computations with triaxial case study, J. Mech. Phys. Solids 91 (2016) 1–13, https://doi.org/10.1016/j.jmps.2016.02.021.
[18] I. Vlahinić, R. Kawamoto, E. Andò, G. Viggiani, J.E. Andrade, From computed tomography to mechanics of granular materials via level set bridge, Acta Geotech. 12 (2016) 85–95, https://doi.org/10.1007/s11440-016-0491-3.
[19] J. Fonseca, C. O'Sullivan, M.R. Coop, P.D. Lee, Quantifying the evolution of soil fabric during shearing using directional parameters, Géotechnique. 63 (2013) 487–499, https://doi.org/10.1680/geot.12.P.003.
[20] M.F. Alam, A. Haque, P.G. Ranjith, A study of the particle-level fabric and morphology of granular soils under one-dimensional compression using insitu X-ray CT imaging, Materials (Basel) 11 (2018) 16–18, https://doi.org/10.3390/ma11060919.
[21] W.H. Imseeh, A.M. Druckrey, K.A. Alshibli, 3D experimental quantification of fabric and fabric evolution of sheared granular materials using synchrotron micro-computed tomography, Granul. Matter 20 (2018) 1–28, https://doi.org/10.1007/s10035-018-0798-x.
[22] A. Al Mahbub, A. Haque, X-ray computed tomography imaging of the microstructure of sand particles subjected to high pressure one-dimensional compression, Materials (Basel) 9 (2016) 7–15, https://doi.org/10.3390/ma9110890.
[23] I. Soriano, E. Ibraim, E. Andò, A. Diambra, T. Laurencin, P. Moro, G. Viggiani, 3D fibre architecture of fibre-reinforced sand, Granul. Matter 19 (2017) 1–14, https://doi.org/10.1007/s10035-017-0760-3.
[24] M.B. Cil, K.A. Alshibli, 3D evolution of sand fracture under 1D compression, Géotechnique. 64 (2014) 351–364.
[25] M.B. Cil, K.A. Alshibli, P. Kenesei, 3D experimental measurement of lattice strain and fracture behavior of sand particles using synchrotron X-ray diffraction and tomography, J. Geotech. Geoenviron. Eng. 143 (2017) 1–18, https://doi.org/10.1061/(ASCE)GT.1943-5606.0001737.
[26] M. Wiebicke, E. Andò, G. Viggiani, I. Herle, Towards the measurement of fabric in granular materials with x-ray tomography, 6th Int. Symp. Deform. Charact. Geomaterials, Buenos Aires, Argentinia, 2015.
[27] M. Wiebicke, E. Ando, I. Herle, G. Viggiani, On the metrology of interparticle contacts in sand from x-ray tomography images, Meas. Sci. Technol. 28 (2017) https://doi.org/10.1088/1361-6501/aa8dbf.
[28] N. Otsu, A threshold selection method from gray-level histograms, IEEE Trans. Syst. Man. Cybern. 9 (1979) 62–66.
[29] J. Zheng, R.D. Hryciw, Segmentation of contacting soil particles in images by modified watershed analysis, Comput. Geotech. 73 (2016) 142–152, https://doi.org/10.1016/j.compgeo.2015.11.025.
[30] M. Faessel, D. Jeulin, Segmentation of 3D microtomographic images of granular materials with the stochastic watershed, J. Microsc. 239 (2010) 17–31, https://doi.org/10.1111/j.1365-2818.2009.03349.x.
[31] M.F. Alam, A. Haque, A new cluster analysis-marker-controlled watershed method for separating particles of granular soils, Materials (Basel) 10 (2017) https://doi.org/10.3390/ma10101195.
[32] N.A. Riley, Projection sphericity, SEPM J. Sediment. Res. 11 (1941) https://doi.org/10.1306/d426910c-2b26-11d7-8648000102c1865d.
[33] H. Wadell, Volume, shape, and roundness of quartz particles, J. Geol. 43 (1935) 250–280, https://doi.org/10.1086/624298.
[34] J. Zheng, R.D. Hryciw, Traditional soil particle sphericity, roundness and surface roughness by computational geometry, Géotechnique. 65 (2015) 494–506, https://doi.org/10.1680/geot.14.P.192.
[35] J. Zheng, R.D. Hryciw, Roundness and sphericity of soil particles in assemblies by computational geometry, J. Comput. Civ. Eng. 30 (2016) 1–13, https://doi.org/10.1061/(ASCE)CP.1943-5487.0000578 (04016021).